Many-body and anisotropy effects in x-ray absorption spectra of pristine and defective vanadium pentoxide

Yu Fujikata⊙

Graduate School of Science and Engineering, Chiba University, Chiba 263-8522, Japan

Fukiko Ota

Graduate School of Science and Engineering for Education, University of Toyama, Toyama 930-8555, Japan

Keisuke Hatada⊙

Faculty of Science, Academic Assembly, University of Toyama, Toyama 930-8555, Japan

Peter Krüger ⊙*

Graduate School of Science and Engineering, Chiba University, Chiba 263-8522, Japan
and Molecular Chirality Research Center, Chiba University, Chiba 263-8522, Japan

X-ray absorption spectra of vanadium pentoxide (V_2O_5) at the vanadium K and L edges are studied with multiple scattering calculations and good agreement with experiment is obtained when the full-potential and multichannel extensions of multiple scattering theory are used. The spectral shapes are analyzed in terms of the local electronic structure at the vanadium sites and they reveal strong anisotropy and final-state correlation effects. The strong polarization dependence of the spectra is explained by the low-symmetry ligand field and vanadyl bonding. The effect of oxygen vacancies, the major intrinsic defect type of V_2O_5, is investigated. Clear spectral changes are found for vanadium atoms next to an oxygen vacancy, which may serve as a fingerprint of defects in electron energy loss spectroscopy.

I. INTRODUCTION

Vanadium pentoxide (V_2O_5) is an important material for heterogeneous catalysis, e.g., for NO_x reduction [1]. Among the different vanadium oxides, V_2O_5 is the chemically most stable one, with vanadium in its highest oxidation state +5. The presence of oxygen vacancies reduces some V^{5+} cations to V^{4+} and is believed to play an important role for the catalytic activity [2]. Vanadium pentoxide is special among transition-metal oxides because of the fivefold coordination of the metal site and the existence of both single and double metal-oxygen bonds. X-ray absorption spectroscopy (XAS) is a powerful method for identifying oxide phases in chemically complex environments and for in-operando characterization [3]. The crystal and electronic structure of V_2O_5 have been investigated extensively [4–9] and theoretical XAS studies from the major core levels (V-1s, V-2p, O-1s) have been reported [10–16]. However, a systematic and comparative theoretical study of the vanadium K and L edges, which provide rich structural and electronic information, is lacking. These spectra are a challenge for theory because of the low symmetry at the metal site, the large metal-oxygen hybridization, and, in the L-edge case, strong final-state multiplet interactions.

Here we present XAS calculations of V_2O_5 at the vanadium K and $L_{2,3}$ edges in the unifying framework of multiple scattering theory (MST). We show that standard MST, which relies on the muffin-tin potential form and the independent particle approximation (IPA), fails to reproduce the experimental absorption spectra because of strong many-body and anisotropy effects. By using the multichannel [17–19] and the full-potential [20–22] extensions of MST, we obtain good agreement with experiment at both absorption edges. We analyze the spectral shapes in terms of orbital character of the final state and explain the strong polarization dependence of the lowest-energy peaks.

Furthermore, we investigate the effect of oxygen defects on the absorption spectra. Oxygen vacancies are the dominant intrinsic defect type in V_2O_5 and they influence the chemical reactivity and catalytic performance [2]. The presence of an O vacancy modifies the geometrical and electronic structure at the neighboring metal sites. This leads to clear changes of the vanadium core-level spectra, which should be measurable with atomically resolved electron loss spectroscopy [23,24].

II. CRYSTAL AND ELECTRONIC STRUCTURE

V_2O_5 has an orthorhombic crystal structure (space group *Pmmn*) with lattice constants $a = 11.512$ Å, $b = 3.564$ Å, and $c = 4.368$ Å [8]. The unit cell, containing two formula units, is shown in Fig. 1. All vanadium atoms are equivalent,
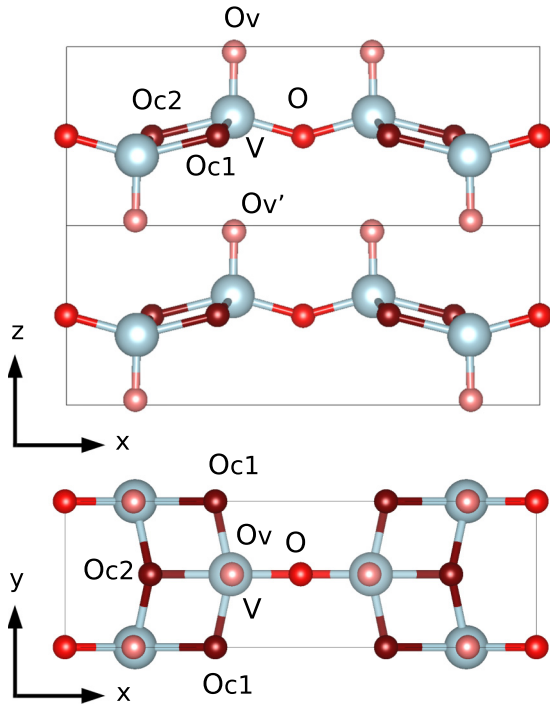
*pkruger@chiba-u.jp

FIG. 1. Top and side view of the V_2O_5 unit cell. Vanadium is shown as large, light-blue balls and oxygen as small red balls. Vanadyl (O_v), chain (O_c), and bridge oxygen (O_b) sites are colored in light, medium, and dark red, respectively. "V" labels the absorber site. As atomic vacancies, the sites O_{c1} and O_{c2} become inequivalent.

FIG. 2. Vanadium $3d$-orbital density of states of V_2O_5. (a) Ground-state potential. (b) Core-hole potential. The d_{xy} DOS is scaled by a factor of $1/3$ for clarity.

but there are three different oxygen sites, named vanadyl (O_v), chain (O_c), and bridge oxygen (O_b). In all vanadium oxides, the cations are located at octahedral sites, but in the case of V_2O_5, the octahedra are so strongly distorted that the local structure is better described as a pyramidal VO_5 coordination. Indeed, along the z axis, the vanadium atom makes one vanadyl double bond V–O_v of bond length 1.58 Å. On the opposite side of the octahedron, the V–$O_{v'}$ distance is very large (2.79 Å) and corresponds to a van der Waals–type bond. The weak out-of-plane bonding makes V_2O_5 a layered material.

In order to generate potentials for the L-edge spectra calculation, we have computed the electronic structure of V_2O_5 in the local density approximation (LDA) using the linear muffin-tin orbital (LMTO) method [25] in the atomic-sphere approximation with 17 empty spheres per V_2O_5 formula unit. The LMTO bands (see Supplemental Material [26]) agree well with other LDA results [7]. Apart from the well-known underestimation of the band gap in the LDA, the band structure is very similar to that of quasiparticle calculations [9]. Figure 2 shows the calculated V-$3d$ partial density of states (DOS) above the Fermi level. The DOS is different for each of the five V-$3d$ orbitals, reflecting the orthorhombic symmetry of the crystal, which fully lifts the degeneracy of the $3d$ shell. The lowest 1 eV of the conduction band is of almost pure $3d_{xy}$ character. The next band from 1 to 3 eV has mixed orbital character with dominant yz and zx contribution. The high-energy part (3–6 eV) is made of $x^2 - y^2$ and $3z^2 - r^2$ orbitals, which form σ-type antibonding states with the $2p$ orbitals of the oxygen ligands. Figure 2(b) shows the final-
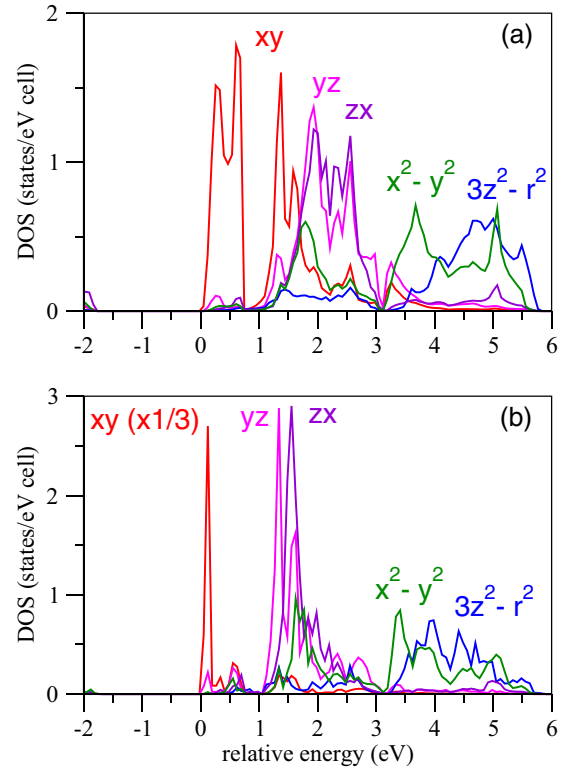
state DOS at the core-hole site, obtained with a full core hole in a $1 \times 2 \times 2$ (56-atom) supercell calculation. With respect to the ground-state DOS [Fig. 2(a)], the energy ordering of the $3d$ partial DOS is maintained, but the centers of the various bands are shifted to lower energy and the t_{2g}-like bands (xy, yz, zx) are much narrower. Remarkably, the xy DOS has become a single sharp line that is well separated from the rest of the $3d$ band. This indicates that the xy orbital localizes as a result of core-hole attraction, and that electrons excited into the xy orbital tend to form a core exciton with the $2p$ hole.

III. $L_{2,3}$-EDGE SPECTRA

The L-edge spectra are computed using the multichannel multiple scattering theory [17–19]. The method features particle-hole configuration interaction at the absorber site through a multichannel scattering matrix. The monopole part of the particle-hole interaction is treated on the one-electron level by using a Kohn-Sham potential, which is a weighted sum of an unscreened part and a fully screened part. The unscreened part is the sum of the ground-state potential and the bare $2p$ core-hole potential. The fully screened potential is obtained as usual, by a self-consistent LDA calculation in a supercell with a core hole at the absorber site. The weight of the unscreened part is $\alpha = 0.1$ as in all our previous studies on metal oxides [18,19,27]. Moreover, as for TiO_2 [19], a potential shift of $\Delta V = +2$ eV is introduced in the calculation of metal d radial waves in order to correct for the underestimation of the band gap in the LDA [19]. The real-space MST calculation is done on a cluster of radius 8 Å, for which the
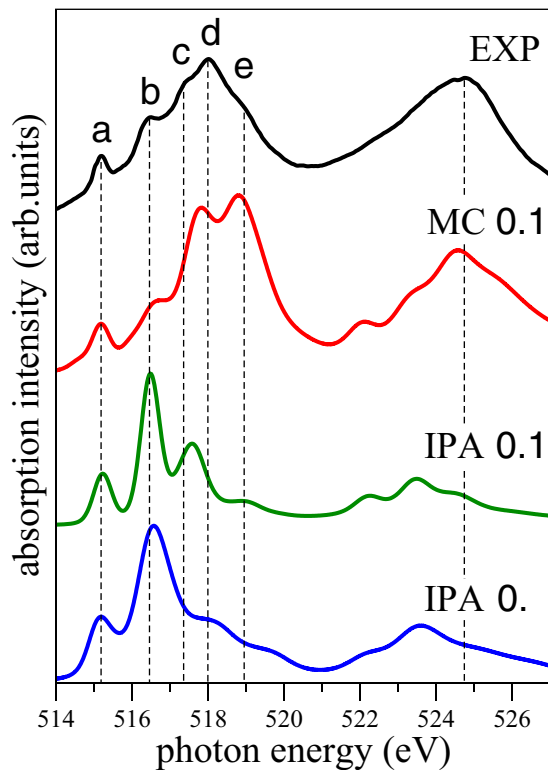
FIG. 3. V-$L_{2,3}$ edge spectra of V_2O_5 calculated with multichannel (MC) theory or in the independent particle approximation (IPA). The α value of the screening model (see text) is 0 or 0.1 as indicated. The experimental spectra (EXP) is taken from [13]. The dotted lines are a guide to the eye.

spectra are found to be well converged in terms of cluster size. In previous XAS studies with quantum chemistry methods [13], it was found that in V_2O_5, the Madelung potential of the point charge embedding converges very slowly with cluster size. Note that the present method does not suffer from such problems because the potential is obtained from a crystal calculation which contains the Madelung potential summed to infinity. As in Ref. [19], the spectra are broadened by convolution with a Gaussian of constant width 0.1 eV and a Lorentzian whose width increases linearly from 0.05 eV at the $L3$ threshold to 0.55 eV at the $L2$ maximum. This energy-dependent broadening can account for the relatively long-lived core-excitonic states below the $L3$ edge and the increased broadening of the $L2$ part due to Coster-Kronig decay and coupling to the continuum. The onset of the spectra is aligned with experiment.

Figure 3 shows L-edge spectra calculated in multichannel (MC) theory in comparison with the IPA and experiment. The MC spectra show a $L3$:$L2$ intensity ratio of about 1.3, which is much closer to the experimental value ($\sim$1.1) than the statistical ratio (2.0) obtained in the IPA. In the IPA, the peak intensities within the $L3$ and the $L2$ features are also very different from experiment, independent of the screening model. In contrast, the peak intensities of the MC calculation agree very well with experiment, except for an overestimation of peak "e." The peak positions are well reproduced in both MC and IPA with $\alpha = 0.1$, except for the "c-d" splitting,
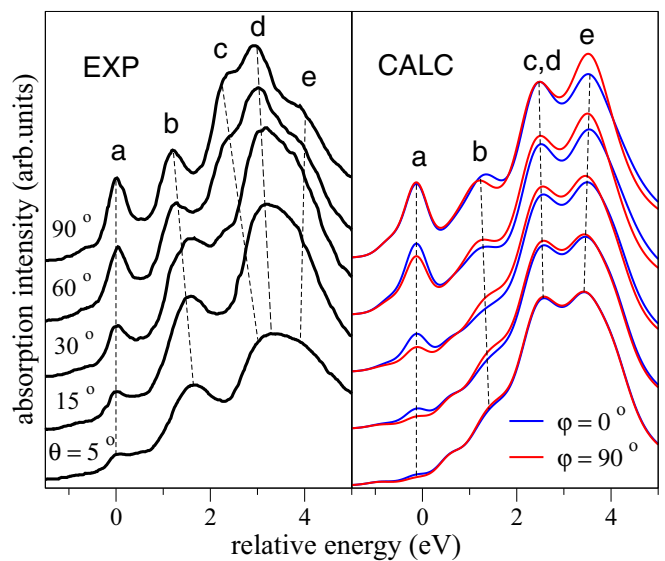

FIG. 4. V-L_3 edge spectra of V_2O_5 for linearly polarized light as a function of polar angle θ between the polarization vector and c axis. Left: Experimental spectra for azimuthal angle $\phi = 90°$ (with respect to the a axis) taken from [28]. Right: Calculated spectra with multichannel theory (blue line: $\phi = 0°$; red line: $\phi = 90°$). The dotted lines are a guide to the eye.

which is missing in both calculations. As seen in Fig. 4, the experimental c-d splitting is largest for in-plane polarization. From this and the energy position (see Fig. 5), the c-d splitting appears to be related to transitions into the $x^2 - y^2$ orbital. As the splitting is absent in both IPA and MC calculations, it is probably due to a shortcoming of the one-electron potential, possibly related to the atomic-sphere approximation used in the LMTO method.

Figure 4 shows vanadium L-edge spectra for linear polarized light as a function of the angle θ between the polarization
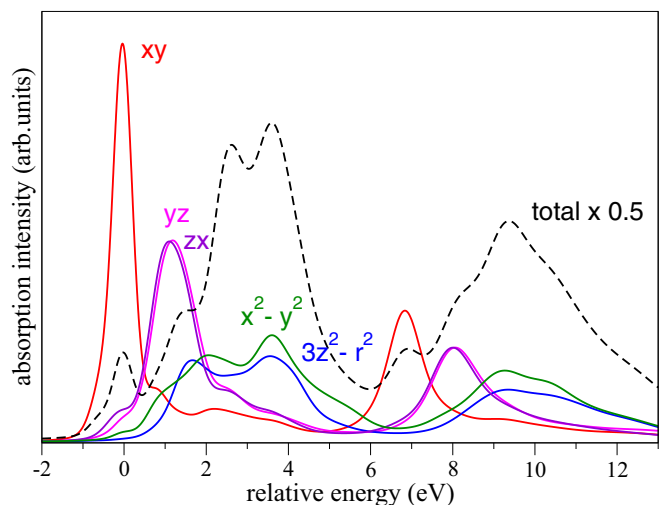

FIG. 5. V_2O_5 vanadium L-edge spectra projected on the final-state V-d orbital symmetries. Note that the five components do not sum up to the full spectrum (dashed lines) because of large interference terms (not shown) caused by particle-hole interaction [19].

vector and the crystal c axis. The experimental data were obtained for an azimuthal angle of $\phi = 90°$ (measured from the a axis). Comparing the calculated spectra for $\phi = 0°$ and $\phi = 90°$, we see that the ϕ dependence is weak, which reflects the approximate fourfold symmetry at the vanadium sites (see Fig. 1). The pronounced θ-angle dependence of the experimental spectra is well reproduced in the calculation. The most remarkable change is seen at peak "a," which is maximum at $\theta = 90°$ and almost vanishes at $\theta = 0°$. Peak "a" may be assigned to final states at the bottom of the conduction band which are of V $3d_{xy}$ character (see Fig. 2). The electric dipole transition intensity from the $2p$ shell to the $3d_{xy}$ orbital varies with θ as $\sin^2\theta$, which explains the observed polarization dependence. The foregoing arguments are based on the one-electron picture, which can be misleading in the case of transition-metal L-edge spectra because of multiplet effects [29]. Figure 5 shows the projection of the particle-hole final states onto V-d orbital symmetries of the excited electron (see Ref. [19] for theoretical details). It can be seen that peak "a" is indeed of almost pure V-d_{xy} character, confirming the assignment based on the single-particle picture. It should be noted that the five d partial spectra in Fig. 5 do not sum up to the total MC spectrum because of large interference terms between the different channels, which are caused by particle-hole coupling [19].

IV. K-EDGE SPECTRA

Metal K-edge spectra are very important for the structural analysis of complex systems and are more bulk sensitive than the L-edge spectra. We calculate the vanadium K-edge spectra using the full-potential multiple scattering (FPMS) code [20,21], which implements MST with non-muffin-tin potentials and space-filling cells. The cell potentials are generated from overlapping free atom charge densities and the real part of the Hedin-Lundqvist potential is used as the optical potential. The spectra are Lorentzian broadened with an energy-dependent width to account for core-hole lifetime and inelastic loss processes [22] and the threshold energy is aligned with experiment. A V_2O_5 cluster of radius 6 Å is used, which contains 20 V atoms, 48 O atoms, and 164 empty cells. The broadened spectra are converged with this cluster size.

Figure 6(a) shows vanadium K-edge spectra for unpolarized light. The experimental data [30] are compared with multiple scattering calculations in full-potential (FP) mode, and in the standard muffin-tin (MT) approximation. In the MT approximation, the space-filling cells are replaced by nonoverlapping spheres with spherically symmetric potential inside, and the empty cells are removed in favor of a constant interstitial potential. The experimental spectrum shows a sharp prepeak (labeled "a" in Fig. 6) and several peaks ("b-e") after the main-edge jump at 5480 eV. All peaks are qualitatively reproduced in both types of calculation. However, the MT spectrum disagrees quite strongly with the data in terms of fine structure and peak intensities, which are much better accounted for in the FP calculation. This comparison highlights the need to use full-potential MST for XAS calculations on crystal structures that are not of the close-packed type [21]. Sipr *et al.* [10] computed the V_2O_5 K-edge spectra with MST in the MT approximation. By comparing different choices
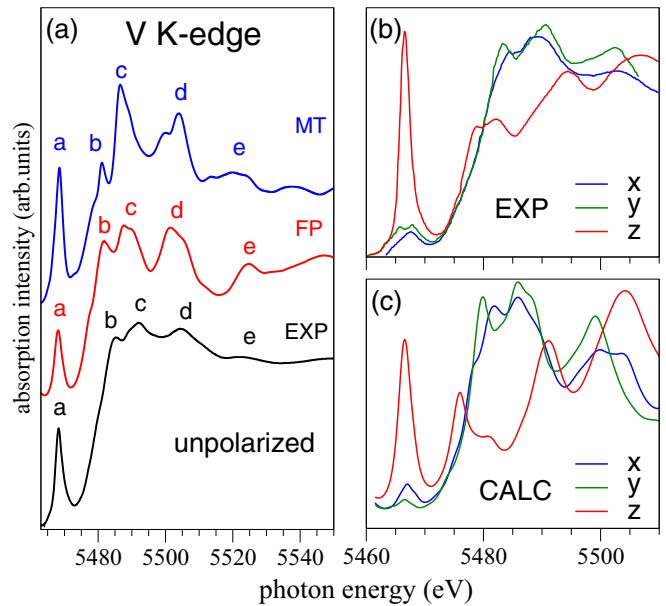

FIG. 6. V-K edge spectra of V_2O_5. (a) Unpolarized spectra. Experiment (Exp) [30] vs multiple scattering calculation in the full-potential (FP) mode and in the muffin-tin (MT) approximation. (b) Experimental spectra for linear polarization [31]. (c) Corresponding theoretical spectra obtained with the FPMS method.

for the muffin-tin radii, they obtained good agreement with experiment. This indicates that the MT approximation can yield satisfactory results even for complex crystal structures, but its predictive power is rather limited.

Figure 6(b) shows the experimental spectra obtained for light that is linearly polarized along one of the three orthorhombic crystal axes. The corresponding FPMS calculation is shown in Fig. 6(c) and the agreement with the data is very good in all cases. While the spectra for x and y polarization are similar, the z-polarized spectrum is very different, reflecting the (001) layered crystal structure. The most striking feature is the prepeak, which is very intense for z polarization but almost absent for x, y polarization. To explain this observation, we look at the unoccupied states of V p symmetry that are probed at the vanadium K edge. Figure 7 shows the unoccupied, vanadium p_x, p_y, p_z and d_{z^2} DOS obtained in a density functional theory (DFT) calculation with the VASP code [32] (see next section for details). In the energy range 2–7 eV, which corresponds to the vanadium K-edge prepeak, the p_z DOS is much larger than the p_x and p_y DOS, and it has virtually the same shape as the d_{z^2} DOS. This shows that the V-d_{z^2} band has a strong admixture ($\sim$25%) of V-p_z states. The prepeak corresponds to the σ^*-type vanadyl bond, made mainly of V-$3d_{z^2}$ and O-$2p_z$ orbitals [33]. The large mixing between V-p_z and V-$3d_{z^2}$ is due to the fact that both orbitals are strongly hybridized with O-$2p_z$ in the vanadyl bond (V=O), which is possible because of the lack of inversion symmetry at the V site (see Fig. 1). If the vanadium atom was in a symmetric bonding configuration, such as O-V-O, then the V-p states would contribute only to *ungerade* molecular orbitals, and V-d states only to *gerade* ones, and so they could not mix.
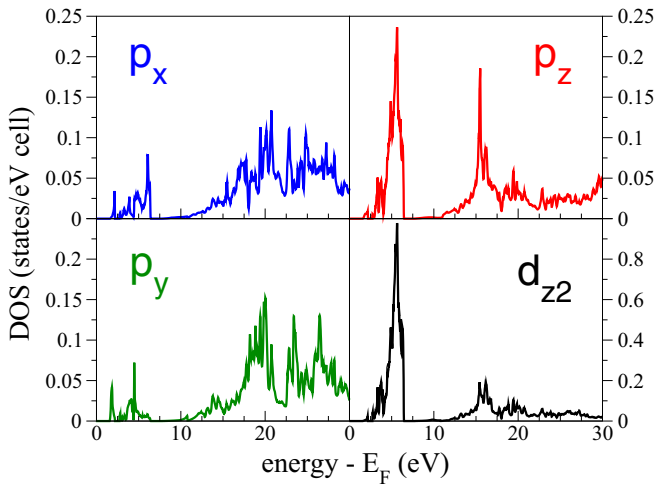
FIG. 7. Partial density of states (DOS) above the Fermi level of V_2O_5 for V-p and V-d_{z^2} states. Note the different vertical scale for d_{z^2}.
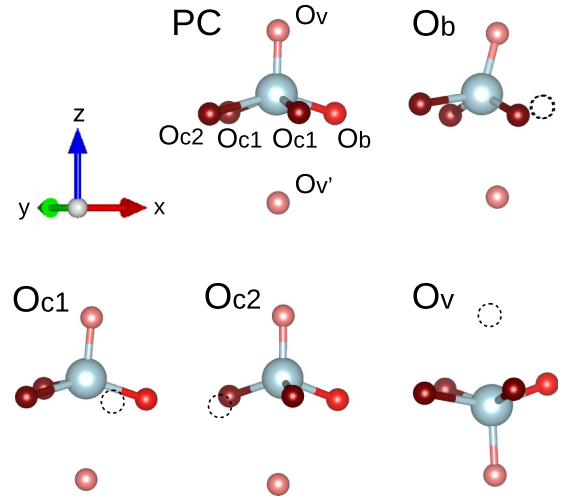

FIG. 8. DFT optimized structure of V_2O_5 around a vanadium atom that is nearest neighbor of an oxygen vacancy (indicated as a dotted circle). The figures are labeled with the vacancy site (see Fig. 1) and PC denotes the perfect crystal.

V. EFFECT OF OXYGEN VACANCIES

We now turn to the effect of oxygen vacancies on the vanadium K- and L-edge spectra. We only consider vanadium sites next to a vacancy. For more distant vanadium sites, the spectral changes are negligible. In order to find the relaxed atomic structure around the oxygen vacancy, we have performed DFT calculations with the Perdew-Burke-Ernzerhof (PBE) exchange-correlation potential and the VASP code [32], which is known for its high structural accuracy. The atomic positions were optimized in a $1 \times 2 \times 2$ supercell with experimental lattice constants, containing one O vacancy. The optimized structure of the defect-free crystal agrees well with previous DFT studies [34] and with the experimental structure, with bond lengths differing from experiment by less than 0.02 Å, except for the vanadyl bond (+0.04 Å). We find that O_v is by far the most stable O vacancy site. Vacancies at O_b or O_c are less stable by 1.68 and 1.89 eV, respectively, in good qualitative agreement with previous DFT studies [8].

The relative stability of the O_v vacancy can be understood from the relaxed structure (see Fig. 8, panel O_v). The loss of a vanadyl bond is partially compensated by the fact that the near-neighbor V atom moves away from the O_v vacancy and makes a new covalent bond with the $O_{v'}$ atom in the lower layer. As a consequence, all vanadium atoms retain a VO_5 coordination. In contrast, when a O_b or O_c vacancy is created, two or three vanadium atoms lose an oxygen bond and become undercoordinated (VO_4) and thus less stable.

The calculated L-edge spectra of vanadium atoms next to an O vacancy are shown in Fig. 9(a) along with the theoretical spectrum of the perfect crystal (PC). The O_b vacancy spectrum is similar to the PC spectrum, except for a shift of the prepeak. With an O_{c1} vacancy, both the prepeak structure and the shape of the L_3-edge main peak are changed, but the overall line shape is also quite similar to the PC spectrum. The O_{c2} spectrum is more strongly modified, especially in the prepeak region. In the case of an O_v vacancy, the spectral changes are most dramatic. The prepeak is gone and both the $L3$

and $L2$ main peaks transform from their roughly triangular shape to a double-hump structure. The finding that the effect is largest for O_v is in line with the fact that the vanadyl V atom is strongly displaced upon O_v vacancy creation. The displacement implies a large modification of the ligand field at the metal site, which is an important factor for L-edge spectral shapes [29]. We conclude that the most stable O vacancy (O_v) has a strong effect on the L-edge spectra of the neighboring vanadium atom, which should be observable with atomic resolution electron energy loss spectroscopy.

Figure 9(b) shows the corresponding vanadium K-edge spectra. There are clear spectral changes for all four O-vacancy types. Interestingly, in the case of an O_v defect, the vanadium K-edge prepeak is split into a doublet. This may be
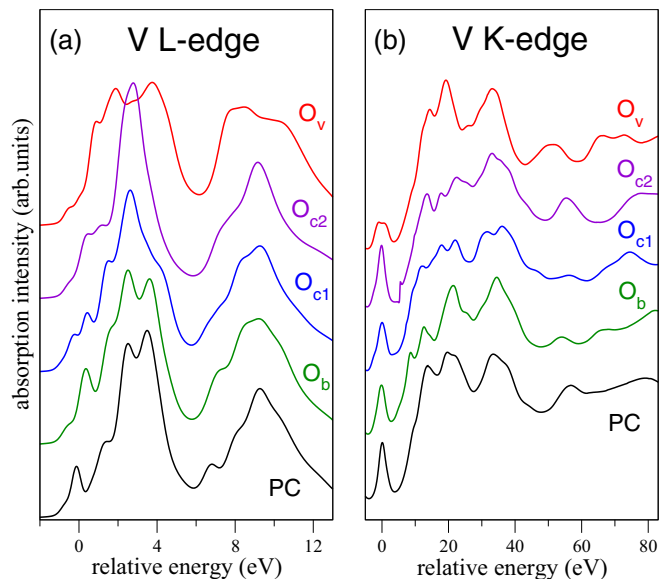

FIG. 9. (a) L-edge and (b) K-edge spectra of vanadium atoms next to an oxygen vacancy at sites O_b, O_{c1}, O_{c2}, and O_v (see Fig. 8) along with the perfect crystal spectrum (PC).

understood from the V-O$_{v'}$-V$'$ structure along z, which results from the V atom relaxation upon O$_v$ vacancy creation; see Fig. 8, panel O$_v$. (V$'$, the regular vanadyl atom in the lower layer, is not shown in the figure.) In this V-O$_{v'}$-V$'$ chain, the V-p_z states on the absorber site V, which determine the K-edge spectra, can couple, via O-2p_z hybridization, to the 3d_{z^2} orbitals of both V and V$'$. These two 3d_{z^2} levels are split in energy because the core-hole attraction pulls down the 3d level on the absorber atom V, but not that of V$'$, which explains the observed splitting of the prepeak. For the other oxygen vacancies, O$_b$, O$_{c1}$, and O$_{c2}$, the prepeak is hardly affected. This again shows that the prepeak is a signature of the vanadyl bond. As far as the main peak is concerned, the situation is rather opposite. While there are clear spectral changes for all defect types, the spectra are less modified for an O$_v$ vacancy than for O$_{c1}$ or O$_{c2}$ defects.

VI. CONCLUSIONS

In summary we have presented a theoretical study of the vanadium K- and L-edge spectra of V$_2$O$_5$ using the full-potential and multichannel extensions to multiple scattering theory (MST). While standard MST yields poor agreement with the experimental data, our extended MST can reproduce the experimental data very well. Both the K- and L-edge spectra display prepeaks with a strong polarization dependence, reflecting the low symmetry of the VO$_5$ coordination. The prepeak at the K edge is due to the large V d_{z^2}-p_z mixing in the vanadyl σ^* bond, and the prepeak at the L edge corresponds to the ligand-field split V-d_{xy} level. Upon formation of oxygen vacancies, the spectra of vanadium atoms next to an O vacancy display substantial changes with respect to the perfect crystal, which should be detectable in atomic resolution spectroscopy.

[1] A. Marberger, D. Ferri, M. Elsener, and O. Kröcher, The significance of Lewis acid sites for the selective catalytic reduction of nitric oxide on vanadium-based catalysts, Angew. Chem. Int. Ed. **55**, 11989 (2016).

[2] J. Haber, M. Witko, and R. Tokarz, Vanadium pentoxide I. Structures and properties, Vanadia catalysts for selective oxidation of hydrocarbons and their derivatives, Appl. Catal. A: General **157**, 3 (1997).

[3] J. Chen, NEXAFS investigations of transition metal oxides, nitrides, carbides, sulfides and other interstitial compounds, Surf. Sci. Rep. **30**, 1 (1997).

[4] W. Lambrecht, B. Djafari-Rouhani, M. Lannoo, and J. Vennik, The energy band structure of V$_2$O$_5$. I. Theoretical approach and band calculations, J. Phys. C: Solid State Phys. **13**, 2485 (1980).

[5] D. W. Bullett, The energy band structure of V$_2$O$_5$: A simpler theoretical approach, J. Phys. C: Solid State Phys. **13**, L595 (1980).

[6] J. C. Parker, D. J. Lam, Y.-N. Xu, and W. Y. Ching, Optical properties of vanadium pentoxide determined from ellipsometry and band-structure calculations, Phys. Rev. B **42**, 5289 (1990).

[7] V. Eyert and K.-H. Höck, Electronic structure of V$_2$O$_5$: Role of octahedral deformations, Phys. Rev. B **57**, 12727 (1998).

[8] S. Laubach, P. C. Schmidt, A. Thißen, F. J. Fernandez-Madrigal, Q.-H. Wu, W. Jaegermann, M. Klemm, and S. Horn, Theoretical and experimental determination of the electronic structure of V$_2$O$_5$, reduced V$_2$O$_{5-x}$ and sodium intercalated NaV$_2$O$_5$, Phys. Chem. Chem. Phys. **9**, 2564 (2007).

[9] C. Bhandari, W. R. L. Lambrecht, and M. van Schilfgaarde, Quasiparticle self-consistent GW calculations of the electronic band structure of bulk and monolayer V$_2$O$_5$, Phys. Rev. B **91**, 125116 (2015).

[10] O. Šipr, A. Šimůnek, S. Bocharov, T. Kirchner, and G. Dräger, Geometric and electronic structure effects in polarized VK-edge absorption near-edge structure spectra of V$_2$O$_5$, Phys. Rev. B **60**, 14115 (1999).

[11] C. Kolczewski and K. Hermann, *Ab initio* DFT cluster studies of angle-resolved NEXAFS spectra for differently coordinated oxygen at the V$_2$O$_5$(010) surface, Surf. Sci. **552**, 98 (2004).

[12] M. G. Brik, K. Ogasawara, H. Ikeno, and I. Tanaka, Fully relativistic calculations of the $L_{2,3}$-edge XANES spectra for vanadium oxides, Eur. Phys. J. B **51**, 345 (2006).

[13] D. Maganas, M. Roemelt, M. Hävecker, A. Trunschke, A. Knop-Gericke, R. Schlögl, and F. Neese, First principles calculations of the structure and V L-edge X-ray absorption spectra of V$_2$O$_5$ using local pair natural orbital coupled cluster theory and spin-orbit coupled configuration interaction approaches, Phys. Chem. Chem. Phys. **15**, 7260 (2013).

[14] G. Fronzoni, R. De Francesco, and M. Stener, $L_{2,3}$ edge photoabsorption spectra of bulk V$_2$O$_5$: A two components relativistic time dependent density functional theory description with finite cluster model, J. Chem. Phys. **137**, 224308 (2012).

[15] R. De Francesco, M. Stener, M. Causà, D. Toffoli, and G. Fronzoni, Time dependent density functional investigation of the near-edge absorption spectra of V$_2$O$_5$, Phys. Chem. Chem. Phys. **8**, 4300 (2006).

[16] G. A. Horrocks, E. J. Braham, Y. Liang, L. R. De Jesus, J. Jude, J. M. Velázquez, D. Prendergast, and S. Banerjee, Vanadium K-edge X-ray absorption spectroscopy as a probe of the heterogeneous lithiation of V$_2$O$_5$: First-principles modeling and principal component analysis, J. Phys. Chem. C **120**, 23922 (2016).

[17] C. R. Natoli, M. Benfatto, C. Brouder, M. F. Ruiz López, and D. L. Foulis, Multichannel multiple-scattering theory with general potentials, Phys. Rev. B **42**, 1944 (1990).

[18] P. Krüger and C. R. Natoli, X-ray absorption spectra at the Ca $L_{2,3}$ edge calculated within multichannel multiple scattering theory, Phys. Rev. B **70**, 245120 (2004).

[19] P. Krüger, Multichannel multiple scattering calculation of $L_{2,3}$-edge spectra of TiO$_2$ and SrTiO$_3$: Importance of multiplet coupling and band structure, Phys. Rev. B **81**, 125121 (2010).

[20] K. Hatada, K. Hayakawa, M. Benfatto, and C. R. Natoli, Full-potential multiple scattering for x-ray spectroscopies, Phys. Rev. B **76**, 060102(R) (2007).

[21] K. Hatada, K. Hayakawa, M. Benfatto, and C. R. Natoli, Full-potential multiple scattering theory with space-filling cells for bound and continuum states, J. Phys.: Condens. Matter **22**, 185501 (2010).

[22] J. Xu, P. Krüger, C. Natoli, K. Hayakawa, Z. Wu, and K. Hatada, X-ray absorption spectra of graphene and graphene oxide by full-potential multiple scattering calculations with self-consistent charge density, Phys. Rev. B **92**, 125408 (2015).

[23] P. Rez, J. Bruley, P. Brohan, M. Payne, and L. Garvie, Review of methods for calculating near edge structure, Ultramicroscopy **59**, 159 (1995), Proceedings of the 2nd international workshop on Electron Energy Loss Spectroscopy and Imaging.

[24] M. Cheynet, S. Pokrant, S. Irsen, and P. Krüger, New fine structures resolved at the ELNES Ti-$L_{2,3}$ edge spectra of anatase and rutile: Comparison between experiment and calculation, Ultramicroscopy **110**, 1046 (2010).

[25] O. K. Andersen and O. Jepsen, Explicit, First-Principles Tight-Binding Theory, Phys. Rev. Lett. **53**, 2571 (1984).

[26] See Supplemental Material at http://link.aps.org/supplemental/10.1103/PhysRevB.101.125124 for the V_2O_5 band structure computed in the local density approximation with the LMTO code.

[27] P. Krüger and C. R. Natoli, Theory of x-ray absorption and linear dichroism at the Ca $L_{2,3}$-edge of $CaCO_3$, J. Phys. Conf. Ser. **712**, 012007 (2016).

[28] E. Goering, O. Müller, M. Klemm, M. L. denBoer, and S. Horn, Angle dependent soft-x-ray absorption spectroscopy of V_2O_5, Philos. Mag. B **75**, 229 (1997).

[29] F. de Groot, Multiplet effects in X-ray spectroscopy, Coord. Chem. Rev. **249**, 31 (2005), Synchrotron radiation in inorganic and bioinorganic chemistry.

[30] S. Yamazoe (private communication).

[31] B. Poumellec, R. Cortes, C. Sanchez, J. Berthon, and C. Fretigny, Polarized xanes and exafs at the V K-edge of $VOPO_4 \cdot 2H_2O$ gel, comparison with the V K-edge in V_2O_5 xerogel, J. Phys. Chem. Solids **54**, 751 (1993).

[32] G. Kresse and J. Furthmüller, Efficient iterative schemes for *ab initio* total-energy calculations using a plane-wave basis set, Phys. Rev. B **54**, 11169 (1996).

[33] H.-J. Zhai, J. Döbler, J. Sauer, and L.-S. Wang, Probing the electronic structure of early transition-metal oxide clusters: Polyhedral cages of $(V_2O_5)_n^-$ ($n = 2$–4) and $(M_2O_5)_2^-$ ($M =$ Nb, Ta), J. Am. Chem. Soc. **129**, 13270 (2007).

[34] X. Yin, A. F ahmi, A. Endou, R. Miura, I. Gunji, R. Yamauchi, M. Kubo, A. Chatterjee, and A. Miyamoto, Periodic density functional study on V_2O_5 bulk and (001) surface, Appl. Surf. Sci. **130-132**, 539 (1998).